CHAPTER 7

Unpatterned Films of $Bi_2Sr_2CaCu_2O_x$

7.1 Introduction

As explained in Sec. 6.1, a critical temperature T_c above the boiling point of liquid nitrogen is desirable for practical applications of high-temperature superconducting films. From the group of high-T_c superconductors matching this requirement, $Bi_2Sr_2CaCu_2O_x$, x∈[8; 9] (Bi2212) is one of the best studied compounds. Within the range of the oxygen content, the optimum oxygenation yields a critical temperature T_c of 85 K. For higher or lower values for x, T_c gradually decreases to values of approx. 54 K [83]. Unlike Y123, however, Bi2212 is a superconductor for the entire x-range and does not become semiconducting or insulating for non-optimal oxygen contents.

Thin films of Bi2212 have been grown by pulsed laser deposition [84], by chemical vapour deposition [85], by solution deposition from PMAA solutions [18] or molten KCl [86], by magnetron sputtering [87], or by a sol-gel process [7].

7.2 Precursor Preparation

$Bi(NO_3)_3{\cdot}5H_2O$, $Sr(NO_3)_2$, $Ca(NO_3)_2{\cdot}4H_2O$, and $Cu(NO_3)_2{\cdot}2.5H_2O$ were dissolved in the stoichiometric ratio 2:2:1:2 in DMF or 2-methoxyethanol. PMAA

(commercial or selfmade) or PAA was added, yielding clear blue or green solutions. With the nitrates:polymer weight ratio of 0.6667:1, the molar ratio 2Bi+2Sr+Ca+2Cu to carboxylic groups was 0.0229:1. The ratio of positive charges from Bi^{3+}, Sr^{2+}, Ca^{2+}, and Cu^{2+} to carboxylic groups was therefore 16 times higher: 0.3670:1.

Precursor solutions were made with low- and high-purity nitrates of Bi, Sr, and Cu. The superconducting films obtained from the different precursors have similar critical temperatures. Critical current densities were, however, only measured for the samples made from the high-purity precursor solutions.

7.3 Film Preparation

As explained in Sec. 2.8, high-T_c superconducting films have to be grown epitaxially $\vec{c}$-axis oriented to obtain high critical current densities j_c. Therefore, $SrTiO_3$ and $LaAlO_3$ (001) substrates were used for Bi2212 films. They were cleaned as described in Sec. 2.4[1] and films were made by spin-casting with 3,000-4,000 r.p.m. After drying on a hot-stage, the samples were heated in an air flow to 820-860 °C.

In analogy to the calculations made for ZnO (Sec. 4.3.2), the shrinkage of the Bi2212 precursor film can be calculated. The thickness of the Bi2212 film should amount 4.8 % of the thickness of the precursor film.

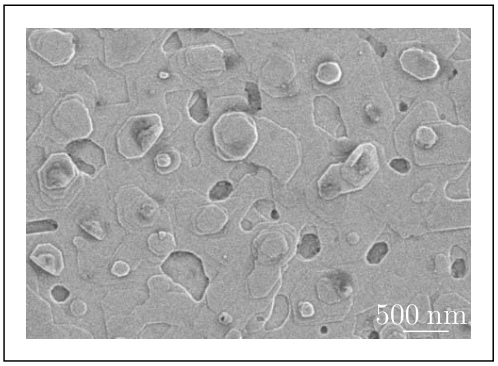

Figure 7.1: SEM image of a ca. 100 nm thick Bi2212 film on $SrTiO_3$ (001).

[1] Alternatively, some substrates were cleaned by heating in air to 900 °C for several hours.

7.4 X-ray Analysis

Fig. 7.1 shows the SEM image of a Bi2212 film on $SrTiO_3$ (001). The film surface has flat smooth terraces with diameters between 100 and 1000 nm. The edges run roughly in four different directions that form mutual angles of 45° and 90°. Two of these directions are parallel to the edges of the substrate, i.e. to the substrate [100] and [010] direction, which become visible at low magnifications of the SEM. This is a first indication for the epitaxial alignment of the film phase. To investigate this phase more closely, ω-2ϑ scans were taken. Fig. 7.2 shows the ω-2ϑ scans of two Bi2212 films on $SrTiO_3$ (001) substrates. Both diffractograms show mainly the (00l) peaks of Bi2212 and $SrTiO_3$. In Fig. 7.2 (b), however, also the peaks of $Bi_2Sr_2CuO_x$ (Bi2201) are present. In addition, the diffractogram also shows unidentified low-intensity peaks. The appearance of Bi2201 in the second sample is probably a consequence of the somewhat deviating stoichiometric composition of the precursor. It is remarkable that the presence of a large amount of a secondary phase does not influence the superconducting properties of the sample in terms of the critical temperarture, as is described below (Sec. 7.6). From the observation that the ω-2ϑ scans show only (00l) peaks it can be concluded that both Bi2212 and Bi2201 were $\vec{c}$-axis oriented. The c lattice parameters of the obtained phases in the two examined samples were determined from the angular position of the (00l) peaks in the ω-2ϑ scans. For Bi2212 they are 30.76(1) Å and 30.70(6) Å in sample 1 and sample 2, respectively. For Bi2201 c=24.40(1) Å.

The lattice parameters a and b of Bi2212 and Bi2201 are approximately by a factor $\sqrt{2}$ larger than a_{SrTiO3}. Therefore, the in-plane orientation of $\vec{c}$-axis oriented Bi2212 (and Bi2201) is a cube-on-cube orientation, where a_{Bi2212} and a_{Bi2201} are parallel to the [110] and [$\bar{1}$10] directions of $SrTiO_3$ or $LaAlO_3$, as depicted in Fig. 2.2. To verify the expected in-plane orientation of the Bi2212 films of this work, texture scans of the Bi2212 {115} reflections were taken. Using the substrate (101) and (002) reflections, the samples were aligned on the 4-circle-diffractometer such that at φ=0° the substrate [100] direction was in the plane of diffraction. The {115} reflections are among the strongest of Bi2212 and do not coincide with any substrate reflections in terms of the d-value. The (115) direction and the $\vec{c}$-axis include an angle of 58.07° in Bi2212. Therefore, in the {115} texture scan of $\vec{c}$-axis oriented Bi2212, the {115} reflections appear at an inclination angle ψ=58.07°. In the case of cube-on-cube growth, the

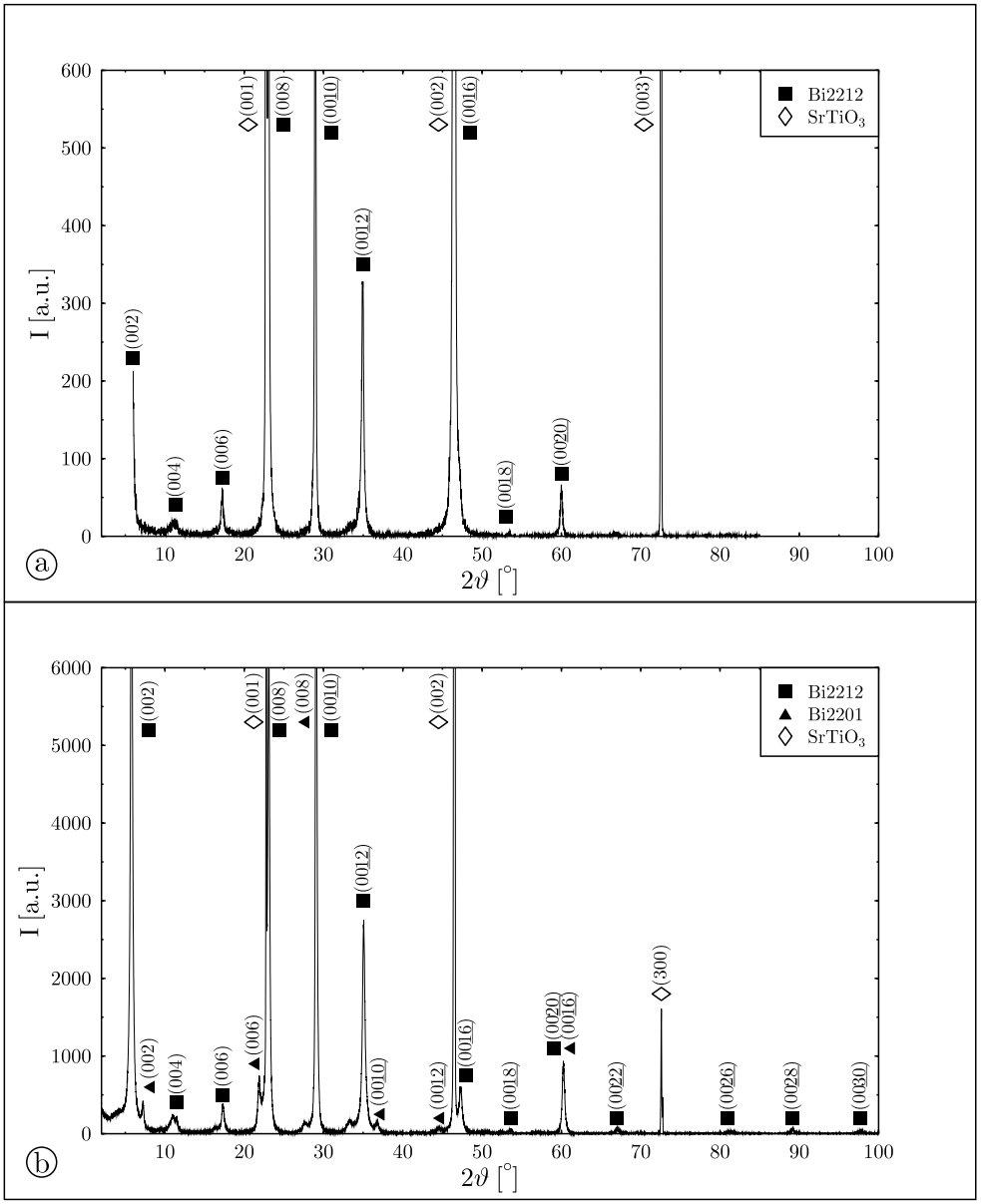

Figure 7.2: ω-2ϑ scans of Bi2212 films on $SrTiO_3$ (001). In (a) only (00l) peaks of Bi2212 and $SrTiO_3$ are visible. In (b) additional (00l) peaks of Bi2201 and unidentified peaks are present.

four peaks appear at the rotational positions φ=0°, 90°, 180°, and 270°. This is the case for the texture scan of sample 2, which is shown in Fig. 7.3. Similarly to $\vec{a}$-axis oriented Y123 (Sec. 6.4), where the $\vec{c}_{Y123}$-axis is parallel to the substrate [100] or [010] directions (because $3 \cdot a_{SrTiO3} \approx c_{Y123}$), Bi2212 domains could exist with $\vec{c}_{Bi2212}$ parallel to the substrate [100] or [010] direction ($c_{Bi2212} \approx 8 \cdot a_{SrTiO3}$). Two out-of-plane orientations for these hypothetical Bi2212 domains are likely: 1. $\vec{a}$ (or $\vec{b}$) along the surface normal. 2. $\vec{a}+\vec{b}$ along the surface normal, which would be epitaxially more favourable, since $\sqrt{2} \cdot a_{Bi2212} \approx 2 \cdot a_{SrTiO3}$. In the {115} texture scan, the peaks of the first hypothetical domain would appear at ψ=90°-58.07°=31.93° and φ=0°, 90°, 180°, and 270°.

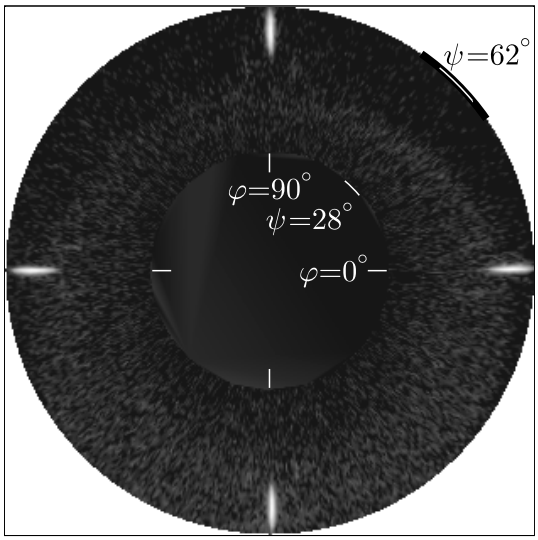

Figure 7.3: {115} texture scan of a Bi2212 film on $SrTiO_3$ (001).

The peaks of the second domain would appear at φ=53.13° and φ=0°±48.60°, 90°±48.60°, 180°±48.60°, and 270°±48.60°. As in Fig. 7.3, none of the {115} texture scans made in this work showed any signs of peaks at these predicted positions.

Once the epitaxial in-plane orientation of the Bi2212 crystallites is confirmed by the texture scans, the crystal faces in Fig. 7.1 can be indexed. A single Bi2212 crystal on a slightly bigger $SrTiO_3$ (001) substrate is schematically shown in Fig. 7.4. The top face, which

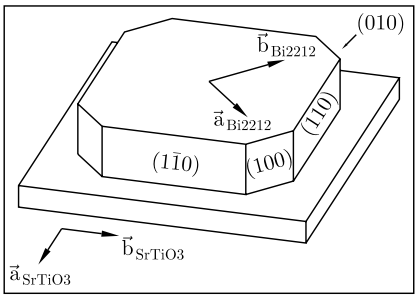

Figure 7.4: Crystal faces of a Bi2212 crystal grown with a cube-on-cube orientation on $SrTiO_3$ (001).

is visible in the SEM images (Fig. 7.1 is the (001) face (pedion). The four different directions of the edges are formed by the (001) face and one of the following eight faces: {100} macropinacoid ((100) and ($\bar{1}$00)); {010} brachypinacoid ((010) and (0$\bar{1}$0)); {110} unit prism ((110), ($\bar{1}$10), (1$\bar{1}$0), and ($\bar{1}\bar{1}$0)). These eight faces are normal to the film plane and therefore not visible in a top-view SEM image.

As the critical current density strongly depends on the epitaxial alignment of the individiual crystallites (Sec. 2.8), rocking curves of the Bi2212 and $SrTiO_3$ (00l) reflections of sample 1 and 2 were taken to quantify the out-of-plane alignment of the Bi2212 phase. The FWHMs of the $SrTiO_3$ (001) and (002) peaks were in the range between 0.5° and 0.8°. For the rocking curves of the film peaks, on the other hand, the angular spread ranged from 0.6° to 1.1°. The mosaic spread of the films was slightly higher than that of the substrate, in contrast to previous reports of equal mosaic spreads of film and substrate [86] (with FWHMs of 0.25°). The in-plane alignment can be quantified by the radial peak widths of the texture scans. For sample 1 and 2 they amount to 1.0°-1.2°, which is larger than the value found by Maréchal et al. [84] (0.6°).

To investigate the in-plane orientation of the Bi2201 domain in sample 2, an area scan of the $SrTiO_3$ $\vec{a}^*\vec{c}^*$-plane was taken, which is shown in Fig. 7.5 (a). All peaks could be identified as (h0l) reflections of $SrTiO_3$ or as (hhl) reflections of Bi2212 or Bi2201. Thereby, the in-plane orientation of Bi2201 was confirmed to be identical to the orientation of Bi2212, i.e. $\vec{a}_{Bi2201} \| [110]_{SrTiO3}$ or $[\bar{1}10]_{SrTiO3}$. Since the investigated reciprocal lattice plane is a high symmetry plane for $SrTiO_3$, any epitaxially grown phase is likely to show reflections in this reciprocal lattice plane. In the scan in Fig. 7.5 (a) there are no traces of sharp peaks other than the identified ones. It is thus very unlikely that a large amount of a phase other than Bi2212 or Bi2201 has grown epitaxially, either in sample 2 or in any other examined sample.

7.5 Superstructure of Bi2212

An area scan of the reciprocal lattice plane $SrTiO_3$ (110)$\vec{c}^*$ of a third sample was also taken (Fig. 7.5 (b)). All strong peaks in the scan could be indentified as (hhl) peaks of $SrTiO_3$ and (h0l) peaks of Bi2212, for even values of h. However, as indicated by the arrows in Fig. 7.5 (b), some of the Bi2212 peaks are surrounded by up to four weak peaks. These satellite peaks, to-

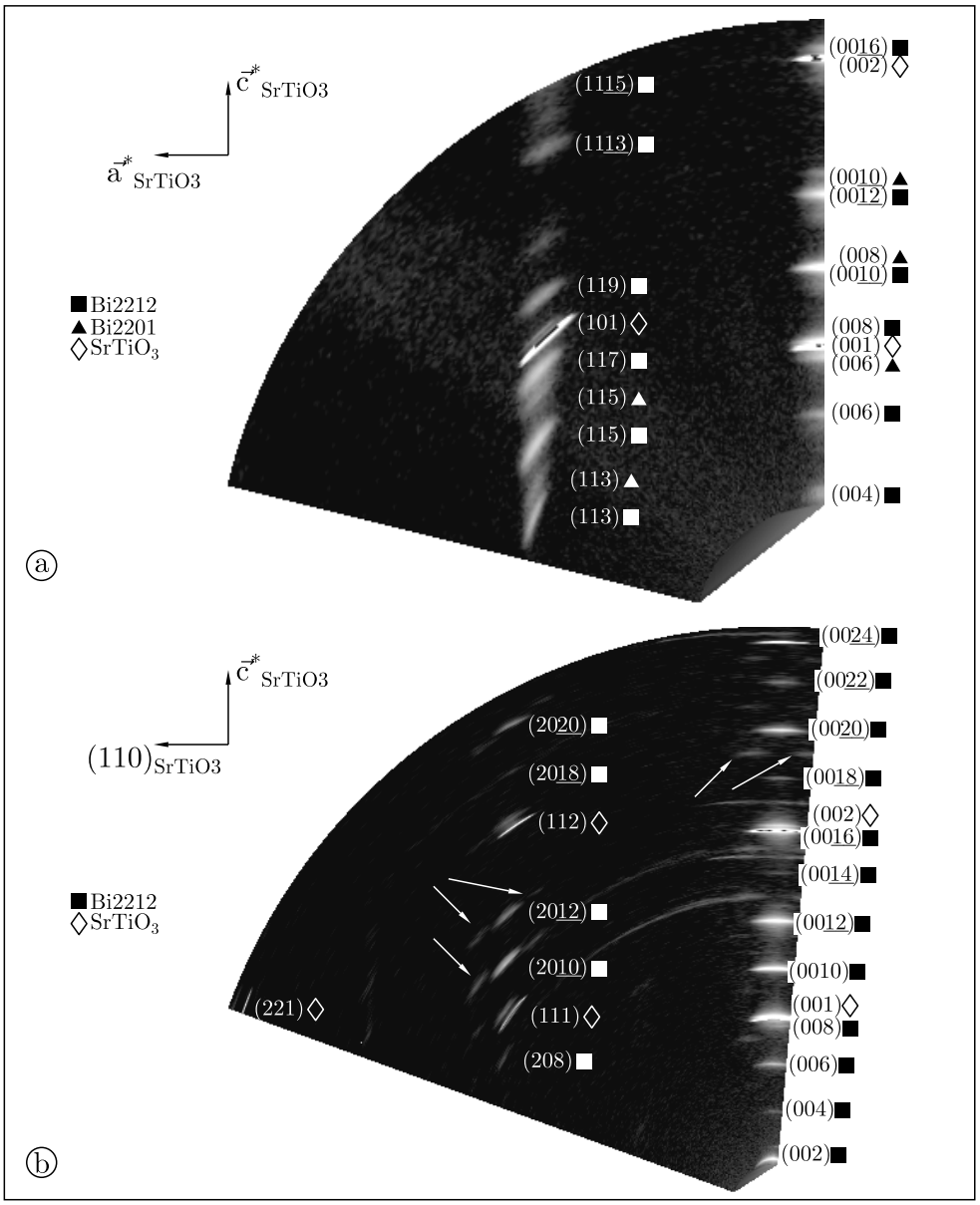

Figure 7.5: Area scans of two reciprocal lattice planes of Bi2212. In (a) the $SrTiO_3$ $\vec{a}^*\vec{c}^*$-plane of sample 2 was scanned ($2\vartheta \in [10°; 50°]$, $\psi \in [0°; 76°]$). In (b) the $SrTiO_3$ $(110)\vec{c}^*$-plane of sample 3 was investigated ($2\vartheta \in [5°; 75°]$, $\psi \in [-5°; 70°]$). The white arrows indicate satellite peaks stemming from the superstructure of Bi2212.

gether with the main peaks of Bi2212, form corner-shared rhombs along the $\vec{c}^*_{Bi2212}$-axis. Due to the elongated shape of the peaks, the vertical spacing of the satellite peaks cannot be measured very precisely. It is on the order of $2c^*$, indicating a periodicity of ca. 30 Å along $\vec{a}_{Bi2212}$ and/or $\vec{b}_{Bi2212}$. Similar satellite peaks have been reported by Hazen et al. [88] from TEM images of Bi2212 crystals. The satellite peaks stem from a superstructure along the $\vec{b}$-axis, due to an incomensurate modulation of the metal ion positions. The periodicty of the superstructure is 4.5b-5b [89, 90]. The fourfold rotational symmetry of the substrate surface leads to the presence of two domains of $\vec{c}$-axis oriented Bi2212, with $\vec{a}_{Bi2212}$ either along $SrTiO_3$ [110] or [$\bar{1}$10]. The area scan in Fig. 7.5 (b) shows therefore not only the Bi2212 (h0l) reflections, but also the coinciding (0hl) reflections and their satellite peaks.

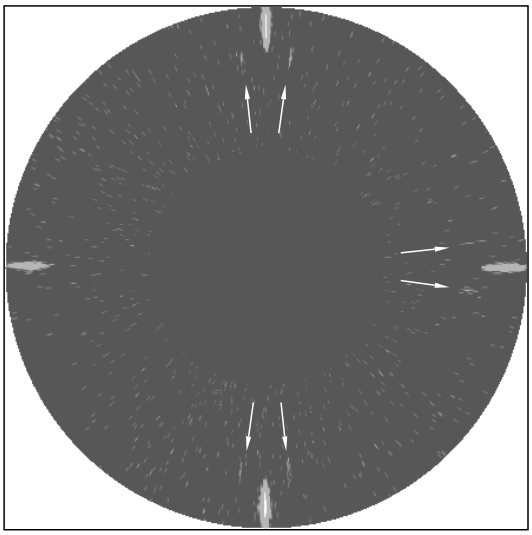

Figure 7.6: Texture scan of the Bi2212 {115} reflections of sample 3. The arrows indicate the satellite peaks surrounding three of the main peaks.

The satellite peaks are also visible in the {115} texture scans, e.g. in Fig. 7.3. Because they are rather smeared out in reciprocal space, they can be discerned in these scans, despite the fact that their d-value is not exactly the same as of Bi2212 {115}. The four {115} peaks are surrounded by pairs of

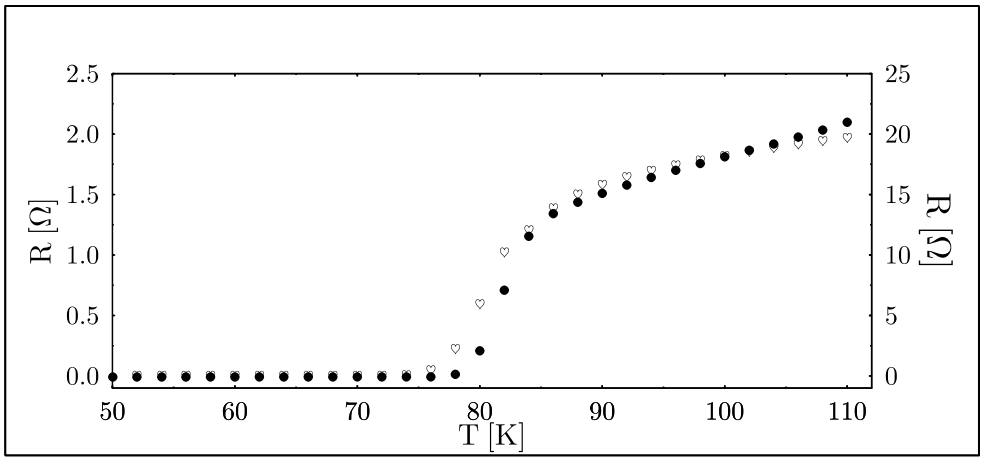

Figure 7.7: Resistance versus temperaure plots of sample 1 (left axis, circles) and sample 2 (right axis, hearts). The critical temperatures, defined by the inflection point of the curve, are 81.6 K and 80.8 K for sample 1 and 2, respectively.

satellite peaks at $\psi \approx 49.5°$. Their positions in φ are approx. $0° \pm 6.5°$, $90° \pm 6.5°$, $100° \pm 6.5°$, and $270° \pm 6.5°$. Fig. 7.6 shows the Bi2212 {115} texture scan of sample 3. The satellite peaks are indicated by arrows.

7.6 Critical Temperatures

The critical temperatures of the Bi2212 films were determined by resistance measurements as described in Sec. 3.3. Fig. 7.7 shows the resistance versus temperature curves of sample 1 and 2. The values for T_c of Bi2212 films measured in this work ranged from 0 K to approx. 85 K.

7.7 Critical Current Densities

Critical current densities j_c were measured for two samples, numbered 4 and 5. This was done by transport measurements (Sec. 3.4.1) in the following way: A narrow conductance bridge that connects two broader contact pads

was etched into the film by means of photolithography. The film was coated with a photoresist, a photomask with the corresponding structure was placed onto the sample and the resist was partially exposed to UV light. The resist was developed and the non-exposed parts were washed off. The remaining part of the resist, in the shape of the conductance bridge and the contact pads, covered the underlying Bi2212 film. The sample was immersed into phosphoric acid for several seconds and the non-covered areas of the Bi2212 film were etched away. Subsequent dissolution of the remaining photoresist exposed the underlying Bi2212 film. Two contacts (source and sense contact) were glued onto each of the pads and the critical current I_c through the bridge was measured as a function of temperature. The critical current was defined as the current, at which a finite voltage ($10\,\mu$V) on the sense contacts was measured. The length of the conductance bridges was $100\,\mu$m and $1000\,\mu$m for sample 4 and 5, respectively. The height of the bridges was approx. 130 nm and 180 nm and their width was $20\,\mu$m and $200\,\mu$m, respectively. The critical current density j_c is the critical current I_c divided by the cross-sectional area of the conductance bridge, height multiplied by width. The results of the j_c measurements are shown in Fig. 7.8.

For sample 5, j_c was additionally measured at the edge of an etched contact pad by the magneto-optical technique (Sec. 3.4.2). The results for three different temperatures and three different external magnetic flux densities are given in Fig. 7.8 in comparison to the results of the transport measurements. The fact that the values of the magneto-optical measurements are higher than those of the transport measurements can be explained in the following way. The magnetooptical method locally determines the critical current density (i.e. at the location of a chosen line profile), while the transport method measures the current density of a larger volume (the conductance bridge), which is likely to contain macroscopic defects such as pores or maloriented grains. Those defects reduce the effective cross-sectional area of the conductance bridge to a value lower than the geometrical cross-section. It is therefore likely that the calculated value of j_c, calculated using the geometrical cross-sectional area, is lower than the real value. For epitaxial Bi2212 films on MgO (001) single crystals, j_c has been found to be as high as 10^5 A/cm^2 at 10 K [91], for polycrystalline thick films ($20\,\mu$m) at the same temperature, a value of $2{\cdot}10^5$ A/cm^2 was reported [92]. Both values are on the same order of magnitude as the values measured for samples 4 and 5.

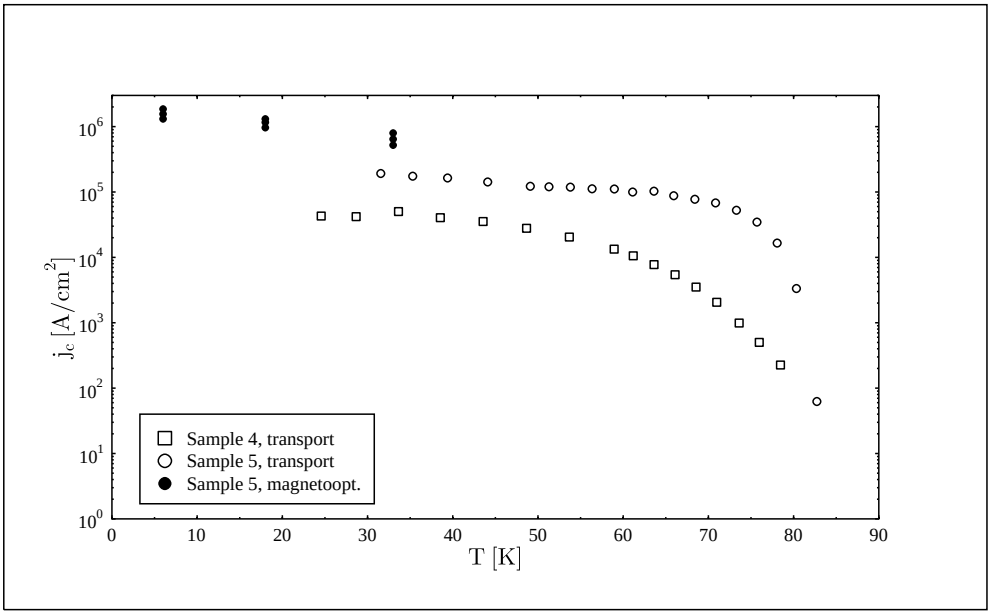

Figure 7.8: j_c as a function of temperature for two Bi2212 films on $SrTiO_3$ (001).

For technical applications high values of both T_c and j_c are desirable. The unpatterned Bi2212 films produced in this work have T_c-values higher than the boiling temperature of liquid nitrogen and they have j_c-values that are comparable to the best films made by technically more complicated methods. The production of Bi2212 films by the solution deposition is therefore an interesting alternative to the conventional methods.